Experimental Assessment of WiMAX Transmissions under Highly Time-Varying Channels

Pedro Suárez-Casal, José Rodríguez-Piñeiro, José A. García-Naya and Luis Castedo
University of A Coruña, SPAIN
{pedro.scasal, j.rpineiro, jagarcia, luis}@udc.es

***Abstract*—Modern wireless communication systems, such as WiMAX, rely on Orthogonal Frequency Division Multiplexing, a very robust modulation against frequency-selectivity, but very sensitive to time-selectivity, which is a typical feature in mobility scenarios. In this work, experimental measurements in real scenarios are carried out by employing WiMAX signals including the standard-compliant pilot signals. Highly time-varying conditions are induced by enlarging the symbol period by time interpolation in the digital domain. In addition, the performance of Inter-Carrier Interference cancellation techniques, which take advantage of the WiMAX pilot structure, are tested to evaluate their behaviour under highly time-varying conditions.**

***Index Terms*—WiMAX; time-varying channels; ICI; OFDM; BEM**

I. Introduction

Most modern wireless communication systems rely on multicarrier schemes such as Orthogonal Frequency Division Multiplexing (OFDM), given their good properties to combat multipath delay. However, OFDM is very sensitive to the distortions caused by highly time-selective channels due to Doppler spreading, which leads to Inter-Carrier Interference (ICI). Channel models which recreate these conditions are widely known in the literature, prominently the Jakes model, and they are useful to validate signal processing techniques under controlled simulation environments. Unfortunately, testing in real-life high-speed scenarios is a challenging task.

ICI estimation and cancellation in OFDM have been studied theoretically, and by simulations using both a single OFDM symbol [1], and multiple OFDM symbols [2], [3], but few works assessed these techniques in real-world scenarios. Some works have shown results of experiments in underwater acoustic communications, where large delays and time variations are easily observed [4]. In the case of wideband communications, it is possible to rely on enlarging the OFDM symbol period to make measurements at low speeds [5]. This technique allows for receiving OFDM symbols affected by large Doppler spreads, without being necessary to make expensive experiments at high speeds. The resulting signal will be less affected by the channel frequency selectivity, but it will provide a framework to test ICI cancellation techniques in real scenarios.

In a previous work, the technique to induce large Doppler spreads was assessed by comparing experimental measurements with simulation results [5]. In this work, the performance of an OFDM receiver that uses several ICI estimation and cancellation techniques is tested by means of experimental measurements in real scenarios. Desired Doppler spread factors are obtained by enlarging the OFDM symbol period.

978-1-4799-5863-4/14/$31.00

II. Signal Processing Chain

The OFDM transmitted signal consists of N subcarriers, which include data symbols as well as pilots and guards. Each WiMAX transmission frame consists of K OFDM symbols. A guard interval is also appended at the beginning of each OFDM symbol by including a cyclic prefix, thus generating symbols of $N_t = N_g + N$ samples. The samples at the output of the DFT are serially transmitted at a sampling rate F_s, producing symbols with time period $T_s = N_t F_s$. The k-th OFDM symbol can be represented as

$$\mathbf{s}_k = \mathbf{G}_1 \mathbf{F}^H \mathbf{x}_k, \tag{1}$$

where $\mathbf{x}_k$ is a $N \times 1$ vector with the transmitted subcarriers, $\mathbf{s}_k$ is a $N_t \times 1$ vector with the transmitted samples, $\mathbf{G}_1$ is a $N_t \times N$ matrix which cyclically extends the symbol, and $\mathbf{F}$ is the standard DFT matrix. The k-th received symbol can be represented as

$$\mathbf{r}_k = \mathbf{F}\mathbf{G}_2(\mathbf{H}_k^{(t)}\mathbf{G}_1\mathbf{F}^H\mathbf{x}_k + \mathbf{n}_k) = \mathbf{H}_k\mathbf{x}_k + \mathbf{w}_k, \tag{2}$$

where $\mathbf{r}_k$ is a $N \times 1$ vector containing the received subcarriers, $\mathbf{G}_2$ a $N_t \times N$ matrix which removes the cyclic prefix, $\mathbf{H}_k^{(t)}$ a $N_t \times N_t$ matrix containing the L-tap channel impulse response affecting $\mathbf{s}_k$, and $\mathbf{n}_k$ a $N_t \times 1$ noise vector with random white Gaussian entries. Also, $\mathbf{H}_k$ is the frequency response of the channel during the k-th symbol, which will contain values different than zero outside the main diagonal if the channel is time-selective, and $\mathbf{w}_k$ is a $N \times 1$ vector of noise variables in the frequency domain with the same properties as $\mathbf{n}_k$, and with variance σ_w^2. Finally, each frame includes a single OFDM preamble symbol at its beginning, used as a reference for detection, as well as timing and frequency offset acquisition.

The Doppler spread observed by an OFDM symbol depends on the normalized Doppler spread, given by $D_n = f_d T$, where f_d is the maximum Doppler frequency, and $T = T_s N$. To adjust the Doppler spread observed, the symbol period can be extended by time interpolation in the digital domain at the expense of reducing the used bandwidth and the effect of channel frequency selectivity. The interpolation factor to be applied before transmission can be expressed as

$$I = \left\lfloor \frac{F_b D_n c}{f_c v N} \right\rfloor, \tag{3}$$

where F_b is the sampling rate of the DACs and ADCs (note that this rate is kept constant during all of our measurements), f_c is the carrier frequency, c the speed of light, v the speed of the mobile where the tests are carried out, and $\lfloor \cdot \rfloor$ the round-down operator. Thus, the symbol period of the OFDM signal actually transmitted by antennas is enlarged by a factor of I, leading to a symbol length for measurements of $T_m = TI$. This interpolation factor is applied in the time domain just before transmission, and this operation is reversed in the received signal before frame detection and synchronization. Further analysis of this technique can be found in previous works [5].

A. Receiver Structure

The receiver performs an initial frame detection on the received signal, and estimates the time and frequency offset. These estimations are done by taking advantage of the correlation properties of the preamble. After compensating for the frequency offset of the frame by multiplying the received signal in the time domain by a complex exponential, the received signal $\mathbf{r}_k$ is processed to estimate the transmitted symbols.

Then, a frequency response estimator is applied to the received frame. Three estimators are considered for the tests: one which assumes that all transmitted subcarriers are known, and another two that rely on the pilot subcarriers embedded in the frequency domain. The estimator which assumes all subcarriers known is an LS estimator in the time-domain. In this case, the vector containing the estimates of the main diagonal of $\mathbf{H}_k$, namely $\mathbf{h}_k$, is obtained as

$$\hat{\mathbf{h}}_k = \mathbf{F}_L(\mathbf{S}^H\mathbf{S})^{-1}\mathbf{S}^H\mathbf{t}_k, \quad (4)$$

where $\mathbf{t}_k = \mathbf{F}^H\mathbf{r}_k$ is a $N \times 1$ vector with the received signal back in the time domain, and $\mathbf{S}$ is a $N \times L$ matrix with the first L columns from a circulant matrix. The first column of such a circulant matrix, is equal to $\mathbf{s}_k$. Finally, $\mathbf{F}_L$ is a $N \times L$ matrix with the first L columns of the DFT matrix.

In the case of the pilot-based channel estimators, a frequency-domain estimator which linearly interpolates coefficients computed at pilot positions in the data subcarriers is used, as well as a mismatched Linear Minimum Mean Squared Error (LMMSE) estimator in the frequency domain assuming that there are P tones reserved as pilot subcarriers, and where only an estimation of the power of the channel coefficients is known, instead of the whole covariance matrix

$$\hat{\mathbf{h}}_k = \mathbf{F}_L(\mathbf{F}_{L,p}^H\mathbf{F}_{L,p} + \sigma_w^2/(E_p\sigma_h^2)\mathbf{I}_L)^{-1}\mathbf{F}_{L,p}^H\mathbf{P}^{-1}\mathbf{r}_k^{(p)}, \quad (5)$$

where $\mathbf{r}_k^{(p)}$ is a $P \times 1$ vector with the entries of $\mathbf{r}_k$ corresponding to the pilot positions; $\mathbf{P}$ is a $P \times P$ matrix with the transmitted pilot symbols in its main diagonal; $\mathbf{F}_{L,p}$ is a $P \times L$ matrix with elements from the DFT matrix, taking its first L columns and its P rows at the positions of the pilot subcarriers; $\mathbf{I}_L$ is the $L \times L$ identity matrix; σ_w^2 is the variance of the noise; σ_h^2 is the variance of the channel coefficients; and E_p is the average power of the pilot symbols (we assume equi-powered pilot subcarriers). In the implemented receiver, the power of the noise is estimated by means of the guard subcarriers not affected by ICI. These estimators were chosen because they can be present in feasible real implementations of a WiMAX receiver, since they do not require the full second-order statistics of the channel.

The output of these frequency response estimators can be used to estimate ICI using groups of M consecutive symbols employing a Basis Expansion Model (BEM) with order P, represented by a matrix $\mathbf{B}$ with dimensions $NM \times P$. The coefficients to use with the BEMs for building the channel matrix can be estimated by

$$\hat{\mathbf{C}}_i = (\mathbf{L}^H\mathbf{L})^{-1}\mathbf{L}^H\mathbf{J}_i, \quad (6)$$

where $\mathbf{J}_i$ is a $M \times N$ matrix which stacks the frequency response estimations of the M symbols of the i-th group, $\mathbf{L} = [\mathbf{b}_{N/2}, \mathbf{b}_{N+N/2}, ..., \mathbf{b}_{(M-1)N+N/2}]^T$ is a $M \times P$ matrix, with $\mathbf{b}_k$ the k-th column of $\mathbf{B}^T$. In our results, $\mathbf{J}_i$ is built from the frequency response estimations obtained with Eqs. (4) and (5). Finally, $\hat{\mathbf{C}}_i$ is a matrix with the coefficients which can be used with $\mathbf{B}$ to compute $\mathbf{H}_k$ in (2) [6].

As a result of this process, an estimation of $\mathbf{H}_k$ is obtained, including the elements outside the main diagonal. This matrix can be used to equalize the received signal and perform symbol detection. In the receiver, a Successive Interference Cancellation (SIC) method is used to remove the ICI, where only the elements of the main diagonal of $\mathbf{H}_k$ are used to equalize and detect the received symbols. Using more elements from the channel matrix besides the main diagonal would reduce the estimation errors [7]. The estimation and equalization algorithm in our setup follows the ensuing steps:

- **Initialization**. ICI is estimated from the first group ($i = 1$) of M OFDM symbols, and removed from the first OFDM symbol to the symbol number $\lfloor M/2 \rfloor + 1$ of the group.
- **Loop**. For $i = 2$ to $i = K - M$, the ICI is estimated from the i-th group of M symbols, and removed from the symbol number $\lfloor M/2 \rfloor + 1$ of the group.
- **Termination**. For $i = K - M + 1$, the ICI is removed from the symbol number $\lfloor M/2 \rfloor + 1$ to the last symbol.

The idea of this structure is to minimize the error of the equalized symbols, given that the ICI estimation error is lower in the central symbols of each block. Once ICI is removed, the same frequency response estimator is run again, since the ICI interference will be lower after this process, and a better estimation can be obtained. Finally, a zero-forcing channel equalization is applied.

III. Experimental Setup

The testbed used for our measurementes is the same as the one in [5], which is based on Ettus USRP B210 [8]. The software of the transmitter and receiver was developed in C++ with Boost and using the Ettus UHD [9], although the scripts to generate the transmitted signals and the channel estimation methods were implemented in Matlab.

In the measurement campaign, the tests were carried out using signals which follow the structure defined for WiMAX

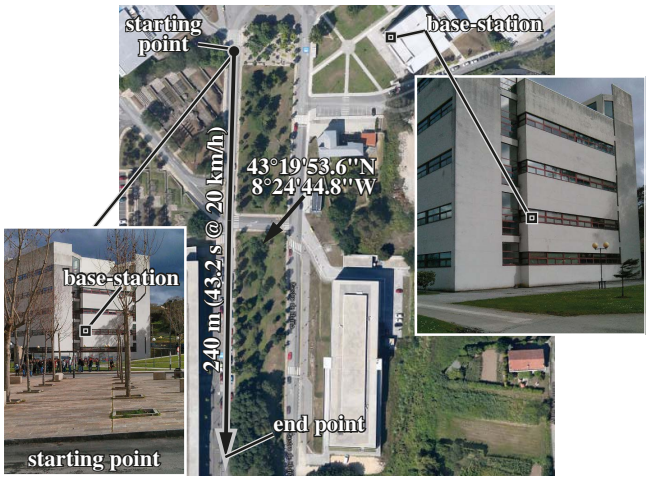

Fig. 1. Measurement scenario in A Coruña, at the University of A Coruña.

downlink [10], using frames with $K = 24$ OFDM symbols, with a unique Partial Usage of Subcarriers (PUSC) zone containing six consecutive bursts, each one occupying four OFDM symbols in the time domain, and all subcarriers in the frequency domain. There are two bursts for each of the valid modulations defined in the WiMAX standard: QPSK, 16-QAM and 64-QAM. The selected WiMAX profile has an OFDM symbol length of $N = 1024$ subcarriers, with a guard interval of 1/8 ($N_g = 128$), and a useful bandwidth of 7 MHz, which requires a sampling rate of $F_b = 8$ MHz. The ICI estimator is configured with groups of $M = 6$ symbols. The carrier frequency is $f_c = 2.6$ GHz, pre-amplified inside the USRP (configured with a gain value of 70 dB out of 89.5 dB), amplified by the Amcom AM003040SF-4H power amplifier [11] (38 dB gain), and finally radiated by the antenna. The power value measured at the antenna input is +18.5 dBm.

The receiver was setup in a car connected to a laptop, with the receive antenna sticked on the roof of the car. The gain of the USRP receiving amplifier is set to 34 dB out of 73 dB to ensure a linear operation. This configuration allows for receiving the signal at the starting point of the course with a peak SNR which exceeds 35 dB. Figure 1 shows the path followed by the car, where at the beginning a strong line-of-sight component is present, but fades away as long as more obstacles stand in the way of transmitter and receiver in the last section of the course.

IV. Experimental Results

In this section, results of measurements of WiMAX downlink transmissions are shown. The tests were carried out using different interpolation factors I to induce different Doppler spread levels. Also, a pilot-based channel estimator, as well as a channel estimator which assumes all transmitted subcarriers are known. An ICI cancellator employing DPS-BEM and KL-BEM, applied for ICI estimation in Eq. (6), was used to test their performance in real scenarios. To measure the performance of the different estimators, Error Vector Magnitude (EVM) values are computed from each burst, measuring the error against the transmitted subcarriers. Moreover, a global estimation of the SNR received during each frame is computed by measuring the signal power in the data subcarriers, and the power of noise in the guard subcarriers not affected by ICI.

In order to ease the visualization of the results, median values of both the EVM and the average SNR are shown. These median values are computed by grouping the frames in clusters dividing the trajectory of the mobile in sections of equal length, and assigning the corresponding median value to that sector. Figures 2 and 3 show results of the perfect estimator and the pilot-based channel estimator respectively, using the ICI estimation method with a DPS-BEM, with order values $P = 3$, $P = 4$ and $P = 5$. The interpolation factor was $I = 32$, hence generating a normalized Doppler spread $D_n = 0.2$, which is equivalent to a speed of 640 km/h in our measurement conditions. It is apparent that the performance of the ICI cancellation process depends on the quality of the initial frequency response estimation. Below a threshold of about 15 dB of EVM before ICI cancellation in the pilot-based estimator, the gain that can be achieved is lower than over this value, being significantly large for values over 17 dB. It is also apparent the gain obtained when higher order BEMs are used, but at lower SNR values, these differences are reduced.

Figure 4 shows the comparison of the performance of the same acquired frames processed with different BEMs, in this case a DPS-BEM and a KL-BEM, again with $I = 32$. It was assumed a Jakes Doppler spectrum when the KL-BEM was computed, since the actual Doppler spectrum of the channel during the measurements was not characterized. Although at $P = 5$ the performance of both estimators is virtually the same, for $P = 3$ a small gain is obtained with the DPS-BEM. This is probably due to a mismatch between the actual Doppler spectrum during the measurements, and the one assumed when the KL-BEM was computed. Also, each frame is used to obtain a different frequency offset and corrected before channel estimation is applied. This frequency offset correction, if not accurate, can affect to the Doppler spectrum observed at the input of the channel estimator. There are methods in the literature to perform joint frequency-offset and channel estimation techniques for OFDM in time-varying scenarios, which could be useful to be used with a KL-BEM [12].

Figure 5 shows the comparison of the performance of the pilot-based estimator with the perfect estimator which uses all transmitted subcarriers as information, using in both cases a DPS-BEM with $P = 5$, and an interpolation factor of $I = 16$, which corresponds to a speed of 320 km/h. In the case of the perfect estimator, it is clear that after ICI cancellation almost all ICI is suppresed, getting very close to the bound defined by the estimated SNR. Comparatively, the pilot-based estimator performs much worse, although at some points with high SNR it gets results better than the perfect estimator which ignores ICI.

Figures 6, 7 and 8 compare the EVM considering the pilot-based estimator, where after ICI cancellation, the decided symbols are used as feedback for a subsequent frequency response estimation using the perfect estimator in which the

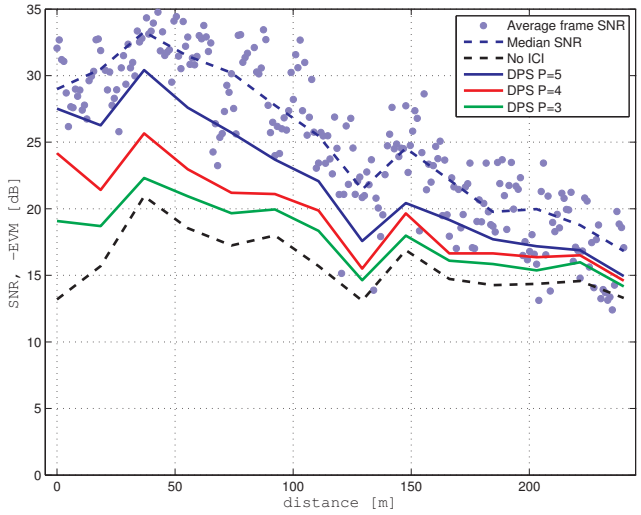

Fig. 2. Perfect channel estimator and DPS-BEM with orders $P = \{3, 4, 5\}$ and with interpolation factor $I = 32$.

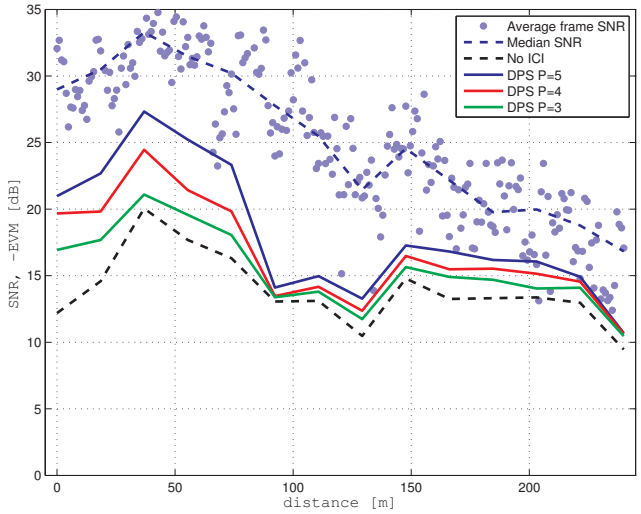

Fig. 3. Pilot-based channel estimator and DPS-BEM with orders $P = \{3, 4, 5\}$ and with interpolation factor $I = 32$.

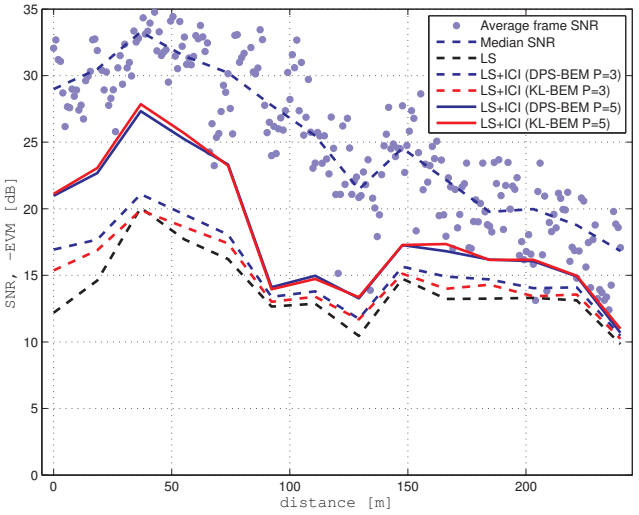

Fig. 4. Pilot-based estimator with DPS-BEM and KL-BEM and interpolation factor $I = 32$.

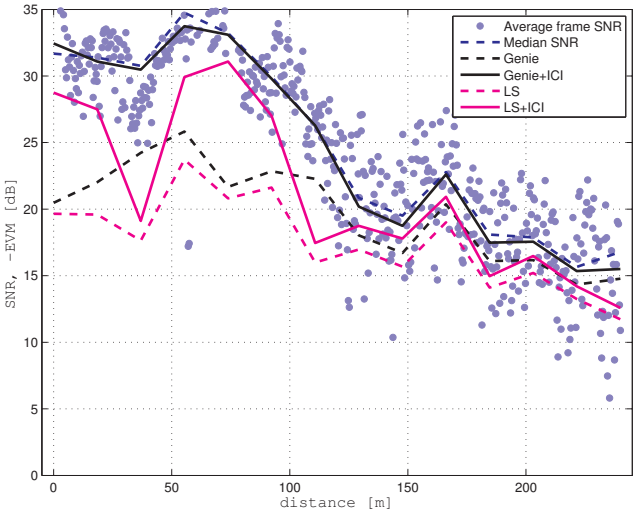

Fig. 5. Comparison of perfect estimator and pilot-based estimator, with interpolation factor $I = 16$.

input consists of pilots as well as the decided symbols. A large gain is observed compared to the estimator which relies only in pilot symbols.

Finally, Fig. 9 shows the performance of the pilot-based estimator with linear interpolation compared to the perfect estimator. Its performance after ICI cancelation is better than the LMMSE estimator at lower SNRs in this case, which can be due to the errors on the edge of the used spectrum which occur in the LMMSE estimator.

V. Conclusions

In this work, measurements of the performance of a WiMAX receiver in a real-world high-speed scenario has been presented, inducing large Doppler spreads by enlarging the OFDM symbol period before transmission, by time interpolation in the digital domain. Results with several channel estimators and ICI cancellators were presented.

These results show that, with the ICI estimator used, the EVM depends not only on the ICI cancellation method, but also on the quality of the initial frequency response estimation. Also, errors in frequency offset estimation can affect this initial frequency response estimation, impairing the performance of the receiver if some Doppler spectrum is assumed. This leads to a negligible gain when a KL-BEM is used, and obtaining even worse results than DPS-BEM for lower BEM orders.

Acknowledgment

This work has been funded by Xunta de Galicia, MINECO of Spain, and FEDER funds of the EU under grants 2012/287, IPT-2011-1034-370000, TEC2010-19545-C04-01, CSD2008-00010, EST13/00272, and FPU12/04139.

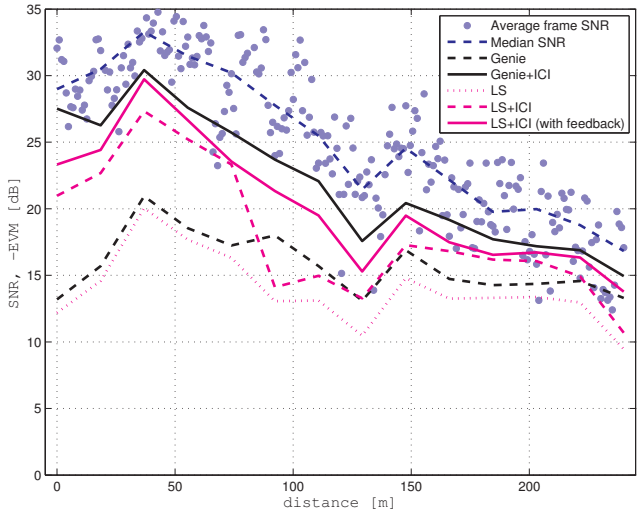

Fig. 6. Comparison of perfect estimator and a pilot-based estimator with feedback, both with interpolation factor $I = 32$.

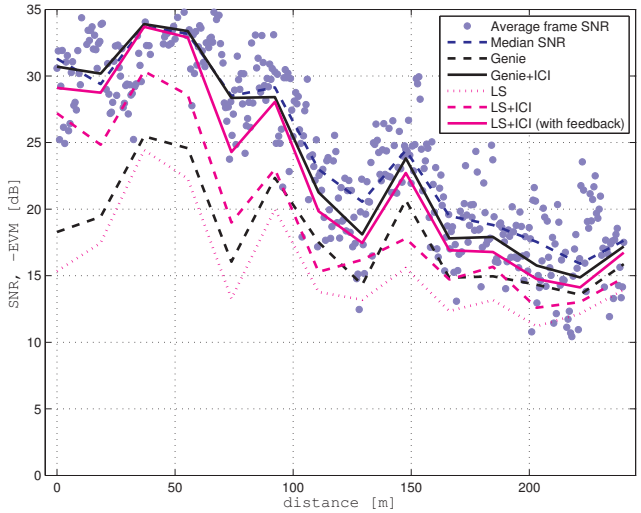

Fig. 7. Comparison of perfect estimator and a pilot-based estimator with feedback, both with interpolation factor $I = 20$.

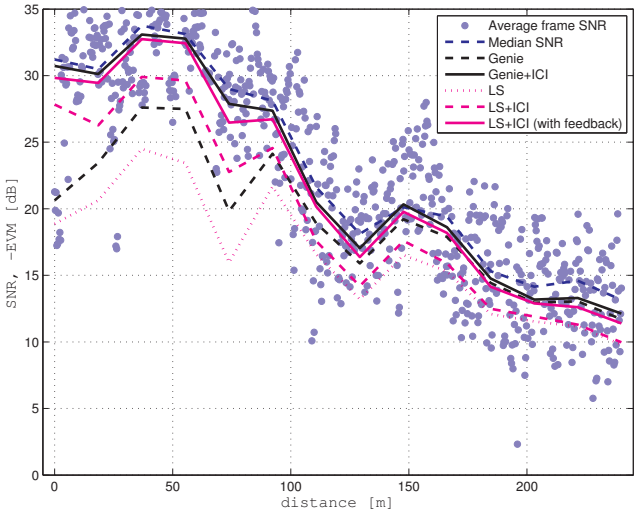

Fig. 8. Comparison of perfect estimator and a pilot-based estimator with feedback, both with interpolation factor $I = 12$.

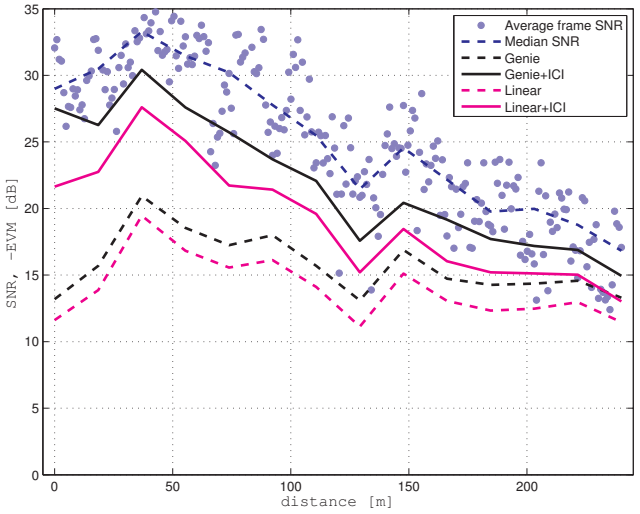

Fig. 9. Comparison of perfect estimator and a pilot-based estimator with linear interpolation, both with interpolation factor $I = 32$.

REFERENCES

[1] Zijian Tang, R.C. Cannizzaro, G. Leus, and P. Banelli, "Pilot-Assisted Time-Varying Channel Estimation for OFDM Systems," *IEEE Transactions on Signal Processing*, vol. 55, no. 5, pp. 2226 –2238, May. 2007.

[2] Zijian Tang, G. Leus, and P. Banelli, "Pilot-Assisted Time-Varying OFDM Channel Estimation Based on Multiple OFDM Symbols," in *IEEE 7th Workshop on Signal Processing Advances in Wireless Communications. SPAWC '06.*, 2006.

[3] H. Hijazi and L. Ros, "Polynomial Estimation of Time-Varying Multipath Gains With Intercarrier Interference Mitigation in OFDM Systems," *IEEE Transactions on Vehicular Technology*, vol. 58, no. 1, pp. 140 –151, Jan. 2009.

[4] G. Palou and M. Stojanovic, "Underwater acoustic MIMO OFDM: An experimental analysis," in *OCEANS 2009, MTS/IEEE Biloxi - Marine Technology for Our Future: Global and Local Challenges*, Oct 2009, pp. 1–8.

[5] José Rodríguez-Piñeiro, Pedro Suárez-Casal, José A. García-Naya, Luis Castedo, César Briso-Rodríguez, and J. Ignacio Alonso-Montes, ," in *IEEE 8th Sensor Array and Multichannel Signal Processing Workshop, 2014. SAM 2014*.

[6] M. Simko, C. Mehlführer, T. Zemen, and M. Rupp, "Inter-Carrier Interference Estimation in MIMO OFDM Systems with Arbitrary Pilot Structure," in *IEEE 73rd Vehicular Technology Conference (VTC Spring), 2011*, May. 2011.

[7] Xiaodong Cai and G.B. Giannakis, "Bounding performance and suppressing intercarrier interference in wireless mobile OFDM," *IEEE Transactions on Communications*, vol. 51, no. 12, pp. 2047–2056, Dec 2003.

[8] "Ettus USRP B210," .

[9] "USRP Hardware Driver (UHD)," .

[10] "IEEE Standard for Local and metropolitan area networks Part 16: Air Interface for Broadband Wireless Access Systems," *IEEE Std 802.16-2009 (Revision of IEEE Std 802.16-2004)*, pp. 1 –2080, 29 2009.

[11] "Amcom AM003040SF4H," .

[12] Hung Nguyen-Le and Tho Le-Ngoc, "Joint Synchronization and Channel Estimation for OFDM Transmissions over Doubly Selective Channels," in *IEEE International Conference on Communications, 2009. ICC '09.*, June 2009, pp. 1–5.